Iranian Journal of Materials Science and Engineering, Vol. 20, Number 3, September 2023
RESEARCH PAPER

A Facile Synthesis of Metallic (Zn and Co) Ferrite Nanostructures as Efficient Solid Photocatalysts for Degradation of Methyl Orange and Methylene Blue under Sunlight

Salihah Hussain Alkhobrani[1], Hossein Bayahia[1], Fares Thabet Alshorifi[2,3,*]

***** *prof.alshorififares@gmail.com, ummod07@hotmail.com*

[1] Department of Chemistry, Faculty of Science, AlBaha University, AL Baha, Saudia Arabia
[2] Department of Chemistry, Faculty of Education and Science, University of Saba region, Yemen
[3] Department of Chemistry, Faculty of Science, Sana'a University, Yemen

Received: June 2023 **Revised: August 2023** **Accepted: September 2023**
DOI: 10.22068/ijmse.3284

Abstract: *In this study, $CoFe_2O_4$ (CoF) and $ZnFe_2O_4$ (ZnF) photocatalysts were successfully prepared by a facile and simple chemical precipitation method for the degradation of methylene blue (MB) and methyl orange (MO) dyes under direct sunlight irradiation. The obtained ferrites were then characterized through XRD, TEM, EDS, UV-vis, and SEM. XRD and TEM results exhibited cubic nanostructures with sizes ranging from 9 to 16 nm and 11 to 18 nm for ZnF and CoF, respectively. SEM images showed homogenous, porous flat surfaces. EDS spectra confirmed the successful synthesis of ZnF and CoF nanostructures with high purity. UV-vis spectra results of MB and MO dyes showed maximum sunlight absorbance in the absence of ZnF and CoF, while a regular decrease in the sunlight absorbance was observed in the presence of ZnF and CoF within 15-60 min. The UV-vis results also showed that ZnF had higher photocatalytic activity than CoF. The experimental findings showed that the highest % degradation was 92.89% and 96.89% for MO and MB dyes, respectively, over ZnF compared to CoF photocatalyst (87.55% and 88.41% for MO and MB, respectively). These findings confirm that porous ZnF and CoF nanostructures are critical in promoting the degradation of dyes under sunlight instead of UV-vis light lamps that consume/require electrical energy.*

Keywords: *Metallic ferrites, $CoFe_2O_4$, $ZnFe_2O_4$, Photocatalysts, Methyl orange, Methylene blue.*

1. INTRODUCTION

Water resources are becoming increasingly scarce all over the world. The unsustainable use of water and the rising population are two important factors creating huge pressure on water use. Additionally, the problem is exacerbated by the pollution of water sources with pollutants. Major water pollutants include agricultural fertilizers and pesticides, industrial and municipal waste, petroleum, and military-use chemicals. These contaminants are largely composed of organic compounds. While some break down naturally and quickly, others break down slowly or never at all. Organic dyes used in the textile and food industries are significant contributors to environmental pollution due to their non-biodegradability, high toxicity to aquatic life, and carcinogenic effects on humans.

In aqueous solutions, the coloring materials are normally added, and a mordant may be needed to improve the fiber's dye speed. Since both colors and pigments are light, they can only absorb some wavelengths. Dyes are colored since they absorb light (400-700 nm) in the visible spectrum, have at least one chromophore (color group) required, and have a conjugate spectrum [1, 2]. The dyes contain double bonds alternating with single bonds in the compound and have electron resonance-stabilizing power. In the event, these features are absent from the composition of the molecules, the color is lost. In addition to chromospheres, most colors contain auxochromes (color aids) such as carboxylic acid, sulfonic acid, amino acid, and hydroxyl groups. Although they are not responsible for color, they can change the color of a colorant and are most typically used to affect dye solubility.

Coloring has been widely used in the clothing, paper, rubber, plastics, footwear, cosmetics, pharmaceutical, and food industries, generating huge quantities of colored wastewater every year and causing significant environmental problems for natural streams, rivers, and consequently, for public health [3–5]. There are about 100,000 commercially available dyes, with over 7,107 tons of dyestuff produced annually around the world. Textiles, food cosmetics, and paper printing are among the industries that employ these dyes, with the textile industry being the major user of dyes [5–8]. Different treatment

[DOI: 10.22068/ijmse.3284]

techniques have been used to address the aforementioned problems, such as photocatalytic degradation, biodegradation, bioelectrochemical processes, chemical oxidation, adsorption, and electrocoagulation, with no chemical degradation [9–16], to isolate the dyes from wastewater before being released into natural water. However, the photocatalytic degradation technique has been discovered to be a simple and cheap alternative treatment tool to remove colors from water. The photocatalyst/adsorbent of choice material, in this case, is critical to treatment efficacy.

The degradation of dyes under UV-vis light using Co, Ni, Cu, and Zn ferrite nanoparticles (MF NPs) was studied. Ni ferrite showed the highest activity and gave 89%, 92%, and 78% of methylene blue (MB), methyl orange (MO), and methyl red (MO), respectively [17]. $AgFeO_2$ delafossite NPs were prepared and tested for the degradation of MB (92% in an alkaline medium) under sunlight [18]. Cobalt ferrite (CoF) was used for degradation of MB (80%) under UV-vis radiation [19]. The organic pollutants were removed from wastewater using zinc ferrite (ZnF) and CoF as less harmful, more stable, and more effective materials. It has been reported that these materials improve degradation, but it is difficult to improve them for photocatalytic applications [20, 21]. To enhance the photocatalytic performance of ZnF nickel-doping nanocomposites (NCs) for degradation of MB (98% degradation by 30% Ni-doped ZnF) [22]. Ag-$CoFe_2O_4$/rGO exhibited superior rate performance and cycle stability [23]. $NiFe_2O_4$/activated carbon photocatalyst was prepared and exhibited a high % degradation of rhodamine of 99.7% within 90 min under simulated sunlight [24]. Metal oxides can be used as photocatalysts in heterogeneous photocatalysis because they are very effective, easy to make, and can be used in a heterogeneous method that lets them be extracted from water [25–27].

The physical properties of photocatalysts, such as crystal structure, particle size, specific surface area, and band structures have a significant impact on the degradation of dyes [28–31] Investigations showed that some nanosized metal oxides were not valuable for the degradation of dyes under sunlight due to a relatively large band gap, a small surface area, a large particle size, and poor electron/hole separation. Co-photocatalysts, synergistic structures, heterojunction structures, and other methods have all been used to address this problem [9, 32, 33]. Inspired by the above considerations, we seek to break new ground in the field of photocatalysis by presenting as-prepared metallic (Zinc and Cobalt) ferrites as efficient solid photocatalysts with smaller nano sizes and a band structure capable of absorbing sunlight for efficient degradation of organic dyes with removal rates higher than those found in previous investigations. The main objective of the current study is to prepare ZnF and CoF nanostructures and then study the kinetic and photocatalytic degradation of organic MB and MO dyes under sunlight instead of UV-vis light lamps that consume/require electrical energy. In brief, solid data is provided on the photocatalytic performance of CoF and ZnF nanostructures and their potential as effective solid photocatalysts under direct sunlight.

2. EXPERIMENTAL PROCEDURES

2.1. Materials

The chemicals and reagents used are of analytical grade purity and were used without any further purification. Distilled water (D.W.), ferric nitrate $Fe(NO_3)_3.\ 9H_2O$, sodium hydroxide (NaOH), zinc nitrate $Zn(NO_3)_2.\ 6H_2O$, and cobalt nitrate $Co(NO_3)_2.\ 6H_2O$.

2.2. Synthesis of Zinc Ferrite and Cobalt Ferrite Photocatalysts

$Zn(NO_3)_2.\ 6H_2O$ (7.4 mmol, 2.2014 g), and $Fe(NO_3)_3.\ 9H_2O$ (14.8 mmol, 5.9792 g) were each dissolved separately in 40 mL D.W. and combined in a flask with continued stirring for 15 min. Then 6 ml of oleic acid was added. 1 M NaOH solution (45 ml) was added to the mixture until pH 10. The resultant precipitate suspension was concentrated in a water bath at 80°C with continuous stirring for 60 min. Then, the precipitate was centrifuged, washed three times with D.W. and one time with ethanol, and dried at 120°C for 3 h. Finally, the resultant $ZnFe_2O_4$ powder was calcined at 500°C for 5 h [17, 18]. The $CoFe_2O_4$ photocatalyst was synthesized using the same procedures with the addition of cobalt nitrate instead of zinc nitrate [9, 10].

2.3. Characterization of the Photocatalysts

The synthesized $ZnFe_2O_4$ and $CoFe_2O_4$ materials were characterized by X-ray diffraction (XRD), EDX, scanning electron microscopy (SEM), and

[DOI: 10.22068/ijmse.3284]

transmission electron microscopy (TEM). Powder X-ray diffraction patterns of the sample were measured using CuKα radiation by a Schimadzo X-ray diffractometer. The XRD patterns were recorded at a diffraction angle ranging from 10° to 80° with a step of 0.03° and an integration time of 4 seconds per step. TEM and SEM were used to take micrographs of the $ZnFe_2O_4$ and $CoFe_2O_4$ materials using a Philips XL 30 attached to the EDX unit.

2.4. Photocatalytic $ZnFe_2O_4$ and $CoFe_2O_4$ Performance in MB and MO Degradation

In this part of the study, MB and MO dye solutions were mixed with 10 mg of ZnF NPs or CoF photocatalysts and stirred in a dark place for 30 min. After that, the mixture was exposed to sunlight for reaction times. The sample was centrifuged to separate the photocatalyst powder from the solution and then analyzed using a UV-vis analyzer. The photocatalytic activity, kinetics of the degradation of dyes, and adsorption ability of ZnF or CoF NPs were tested for model pollutant MO and MB degradation under sunlight irradiation. Uv-vis spectra were used to determine the concentration of dyes at a wavelength of maximum absorbance of 664 and 464 nm for MB and MO, respectively. The mathematical relationship between the degradation percentage (D%), final concentration (C), and initial concentration (C_o) is:

$$D\% = \frac{C_0 - C}{C_0} * 100 \quad (1)$$

3. RESULTS AND DISCUSSION

3.1. Characterization of Photocatalysts

3.1.1. X-ray diffraction (XRD) measurements

The XRD analysis of the as-prepared CoF and ZnF photocatalysts is shown in Fig. 1. The XRD diffraction pattern of CoF photocatalysts shows the diffraction peaks at 2θ= 18.6 (001), 32.8° (100), 38.01° (101), 50.8° (102), 58.6° (110), 62.07° (111), 68.3° (103) and 72.03° (201), which are consistent with cubic spinel phase (JCPDS card No. 21-1272) [10, 17, 21, 34, 35], indicating the crystalline nature of the synthesized photocatalysts. On the other hand, the same pattern was also obtained for ZnF NPs (the peak pattern of ZnF NPs was similar to the cubic CoF phase), though small shifts toward higher 2θ took place at the 001 and 101 planes due to the Zn concentration, confirming that ZnF NPs were successfully prepared. The XRD diffraction pattern of ZnF NPs can be the index to a cubic spinal phase: JCPDS card No. 28-1042. Compared with the CoF spectrum, the intensity of CoF peaks was lower and weaker, which confirmed the homogeneous synthesis. A new small peak at 2θ= 27.7 was detected only with the ZnF NPs, which corresponds to the 211 plane, it could indicate an increase in the crystallinity of the ZnF NPs. The sharp measured diffraction patterns of the CoF and ZnO curves confirmed that the as-prepared CoF and ZnF are crystalline materials [36, 37]. In addition, no peaks of other impurities were found in the XRD spectra, revealing the high purity of the synthesized photocatalysts. The broad XRD peaks of both CoF and ZnF samples indicate that the as-synthesized CoF NPs and ZnF NPs are nanostructured. The XRD data, which is nearly identical to the TEM results below, provided further evidence for the successful synthesis of CoF and ZnF NPs. The average crystalline size is calculated by the Scherer equation:

$$d = \frac{K\lambda}{\beta \cos\theta} \quad (2)$$

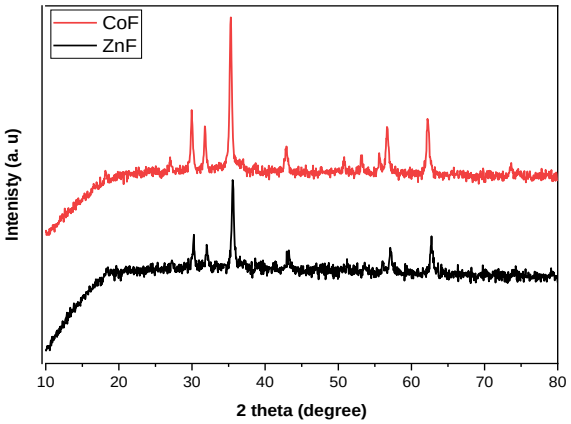

Fig. 1. XRD of ZnF and CoF samples

Where (d) is the size of the particle, K is known as the Scherer's constant (K= 0.94), λ is the X-ray wavelength (1.54178 Å), β is the full width at half maximum (FWHM) of the diffraction peak, and θ is the angle of diffraction. The CoF NPs' nanosize ranged from 11 to 18 nm, while the ZnF NPs' ranged from 9 to 16 nm. According to these results, we conclude that CoF and ZnF NPs may promote the photocatalytic degradation rate of organic dyes. These findings could be the reason for the high photocatalytic performance of ZnF

[DOI: 10.22068/ijmse.3284]

for the MB and MO degradation compared to the CoF photocatalyst.

3.1.2. Energy-dispersive X-ray (EDX) spectroscopy

The chemical composition and purity of ZnF and CoF samples were determined via EDX analysis, as shown in Fig. 2 (a and b). Fig. 2 (a) shows the EDX spectrum of the ZnF sample, which proved the presence of characteristic Fe (24.7%), Zn (55.3%), and O (25.0%) peaks, indicating the as-prepared $ZnFe_2O_4$ with high purity, in good agreement with the TEM and XRD analyses. On the other hand, Fig. 2 (b) shows the EDX spectrum of CoF sample. This figure proved the presence of characteristic Co (58.2%), Fe (23.3%), and O (18.5%) peaks, indicating that $CoFe_2O_4$ NPs were successfully prepared with high purity, in good agreement with the TEM and XRD results. These results provided further evidence for the successful synthesis of CoF NPs and ZnF NPs with high purity.

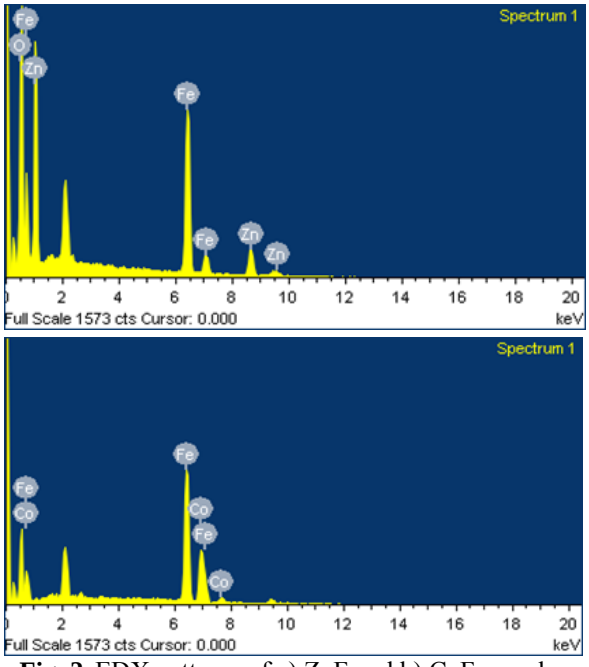

Fig. 2. EDX patterns of a) ZnF and b) CoF samples

3.1.3. Scanning Electron Microscopy (SEM) measurements

SEM analysis of the synthesized ZnF and CoF photocatalysts is shown in Fig. 3 (a and b). This figure shows the differences between the surface morphologies of ZnF and CoF samples. The SEM images showed homogeneous flat surfaces that were porous in nature. It is clear from SEM images that the morphology of the ZnF has a porous flat surface and small spherical NPs in the shape shown in Fig. 3(a), indicating the presence of some ZnF NPs or Zn NPs with very small nano sizes on the surface. On the other hand, the morphology of the CoF photocatalyst also has a porous flat surface with spherical clusters on the surface shown in Fig. 3(b), indicating the presence of some CoF NPs or Co NPs with very small nanosizes on the surface. The surface of CoF has more agglomeration than ZnF, which agrees well with the TEM results. This may be due to the magnetic properties of cobalt ions. Therefore, ZnF nanoparticles were smaller in size than CoF nanoparticles.

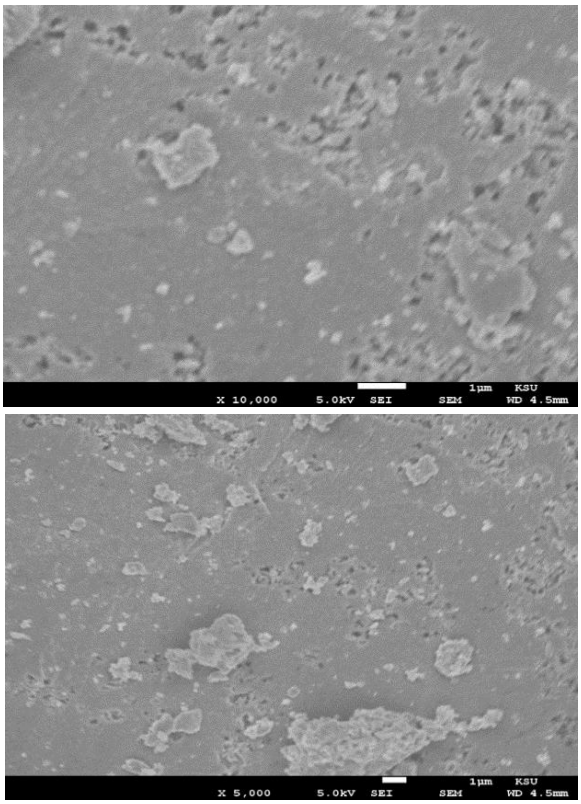

Fig. 3. SEM micrographs for a) ZnF and b) CoF samples.

3.1.4. Transmission electron microscopy (TEM) measurements

The morphology and particle sizes of ZnF NPs and CoF NPs were characterized by TEM and are displayed in Fig. 4 (a and b). The TEM images illustrated differences in the morphologies of the prepared ZnF and CoF photocatalysts. For ZnF and CoF, the micrograph showed some nanowires.

[DOI: 10.22068/ijmse.3284]

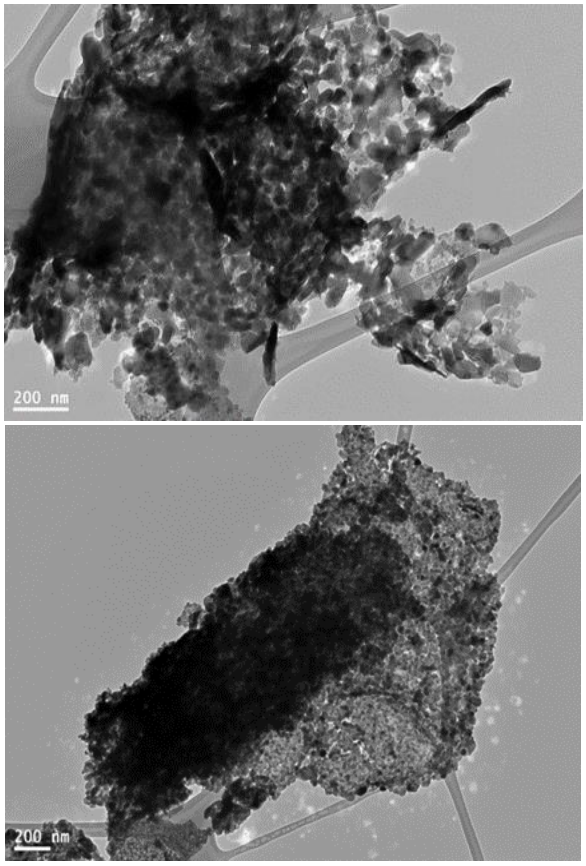

Fig. 4. TEM micrographs for a) ZnF and b) CoF samples

Fig. 4 (a) shows the TEM image of ZnF NPs, which confirms the formation of cubic spinal ZnF nanostructure with particle sizes ranging from 9 to 17 nm. This is in good agreement with the XRD results. While Fig. 4 (b) shows the TEM image of CoF NPs, which confirms the formation of cubic spinal CoF nanostructure with particle sizes ranging from 11 to 19 nm, this agrees well with the XRD results. Furthermore, some agglomeration of $ZnFe_2O_4$ and $CoFe_2O_4$ NPs can be observed as black circles in the center of the TEM images. This is due to the adhesion of the metallic ferrites to each other by weak forces. These results revealed that the CoF morphology has more agglomeration than ZnF. This may be due to the magnetic properties of cobalt ions. On the other hand, TEM images showed that the size of ZnF NPs was smaller than that of CoF NPs. This may be due to the magnetic properties of cobalt ions in the CoF NPs, which led to larger particle sizes and more aggregates compared to the ZnF NPs.

3.2. Application: PhotoCatalytic Activity

3.2.1. Photodegradation of MB and MO dye using ZnF and CoF photocatalysts

The photodegradation of MO and MB dye (10 ppm) over CoF and ZnF photocatalysts (10 mg) under sunlight was carried out. The suspension was agitated with a magnetic stirrer in the dark room for 60 min before the photocatalytic degradation began, and then the reaction setup was exposed to sunlight at the same conditions of photodegradation of MB and MO using CoF and ZnF photocatalysts. For comparison, blank experiments with MB and MO solutions were performed without adding any amount of the prepared photocatalysts. There was no obvious degradation of MB and Mo after 60 min of irradiation without the photocatalyst. The results revealed that no MB (or MO) is destroyed by sunlight without the photocatalysts, showing that MB and MO are relatively stable under irradiation. Figs. 5 and 6 display the UV/visible spectra of MB and MO dyes, respectively, before the photocatalytic degradation processes (without any amount of photocatalysts) and after varying sunlight irradiation time in the presence of CoF NPs or ZnF NPs. The MB and MO dyes showed maximum sunlight absorbance in the absence of CoF NPs and ZnF NPs. In the presence of CoF and ZnF photocatalysts, a regular decrease in the sunlight absorbance was observed at 15-60 min due to photocatalytic degradation of MB and MO dyes under sunlight, indicating successful degradation of the dyes. The longer the exposure time of the sample to sunlight, the greater the photocatalytic degradation of MB and MO dyes. However, ZnF showed higher photocatalytic activity than CoF for MB and MO degradation, which is in good agreement with the experimental photocatalytic degradation. Thus, CoF and ZnF photocatalysts demonstrated high photocatalytic degradation of dyes within 60 min, which is logically reported because dye decomposition can be affected by time. The concentration of the aqueous MB and MO solutions was reduced dramatically and measured using a UV/visible spectrophotometer at 664 nm and 464 nm, respectively. The findings confirmed that porous CoF and ZnF nanostructures were critical in promoting the degradation of MB and MO dyes on the active CoF and ZnF sites and their surface pores during the photocatalytic reaction, resulting in enhanced photocatalytic degradation under

[DOI: 10.22068/ijmse.3284]

sunlight instead of UV-vis light lamps that consume/require electrical energy. This agrees with the research work referenced [21, 35]. In general, the degradation efficiency of MB and MO is considerably increased with time in the presence of photocatalysts [34], where, within 15-60 min, the concentration of MB and MO dyes gradually dropped and reached the maximum degradation rate [36].

3.2.2. Kinetic study of photocatalytic degradation of MB and MO over Zinc ferrite and Cobalt ferrite

Photocatalytic degradation of MB and MO dyes increased with increasing photodegradation time until equilibrium was reached at 60 min, after which the degradation rate remained constant, as shown in Figs. 7 and 8. As a result, 60 min was selected as the ideal time for dye degradation. According to experimental results, the photocatalytic degradation percentage of MB and MO dyes on the as-prepared photocatalysts increased with the increase in photodegradation time, as confirmed by the UV-vis spectra of these dyes. The findings confirmed that the ZnF photocatalyst showed higher photocatalytic activity than the CoF photocatalyst for the degradation of MB and MO dyes. This agrees well with the results of the UV-vis spectra. The highest % degradation was 92.89% and 96.89% for MO and MB, respectively, on the znF photocatalyst compared to the CoF photocatalyst (87.55% and 88.41% for MO and MB, respectively). This could be attributed to the fact that more functional Fe-O and Zn-O groups attached to the ZnF photocatalyst are available to bind more toxic dye, or it could be due to the magnetic properties of CoF NPs, which led to larger particle sizes and larger aggregations than ZnF NPs. This means significantly more photocatalytic active sites and smaller nano sizes (which have a larger surface area) for ZnF NPs, which leads to higher photocatalytic performance in degrading the dyes.

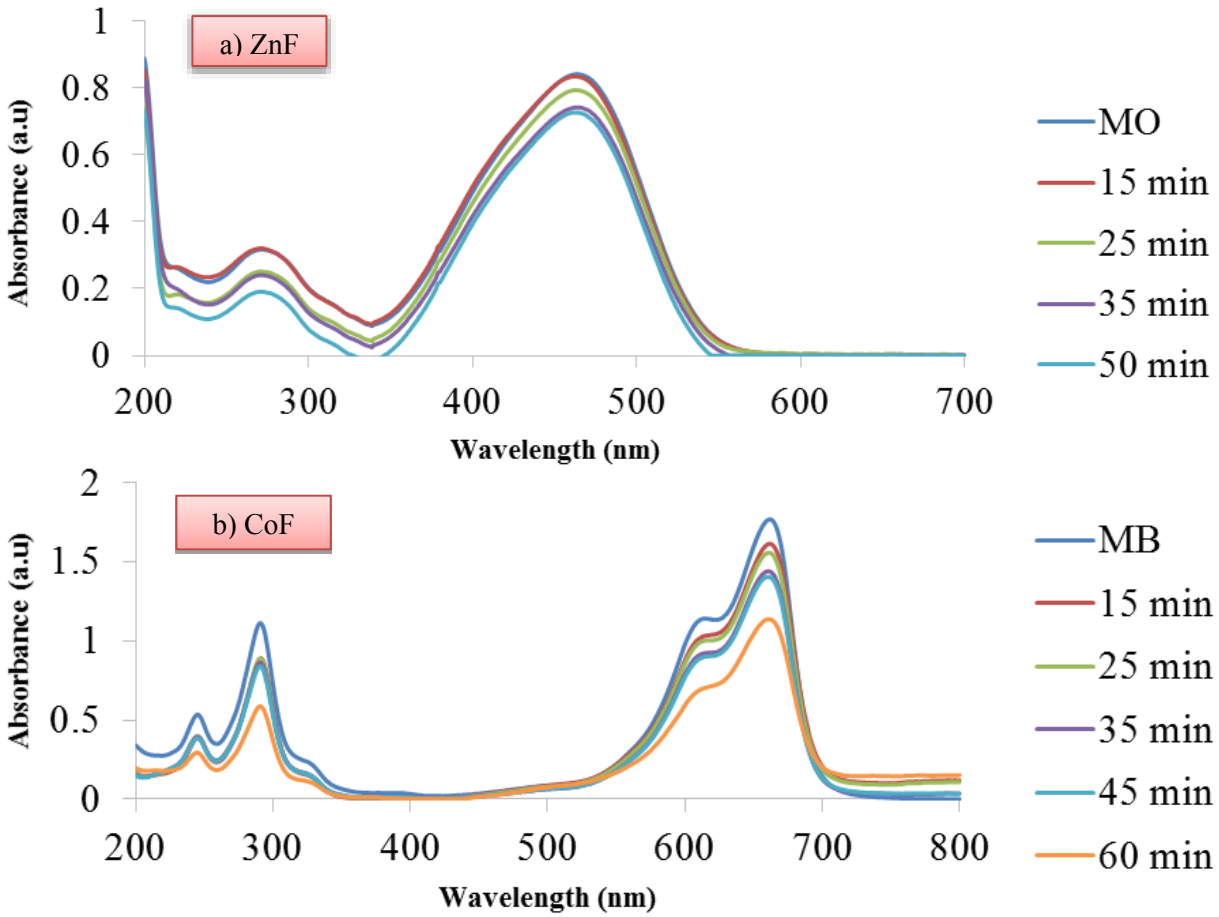

Fig. 5. Typical time-dependent evolution of UV-vis spectra for MB degradation under sunlight by a) ZnF and b) CoF photocatalysts.

[DOI: 10.22068/ijmse.3284]

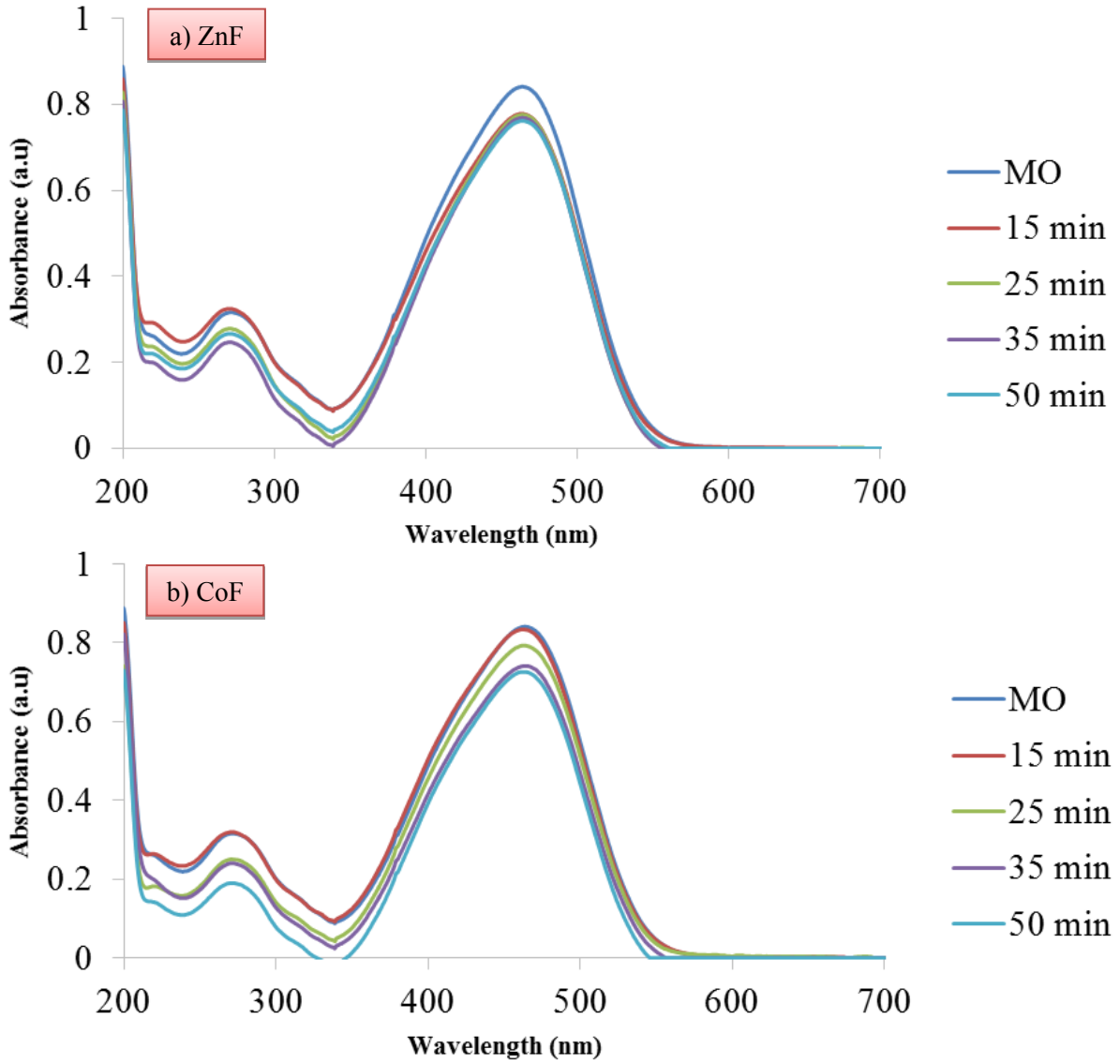

Fig. 6. Typical time-dependent evolution of UV-is spectra for MO degradation under sunlight by a) ZnF and b) CoF photocatalysts

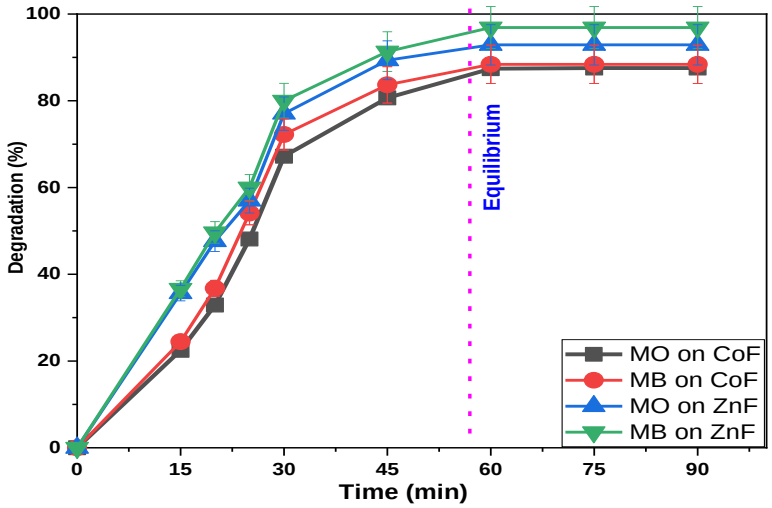

Fig. 7. The degradation rate of MO and MB over CoF and ZnF samples under sunlight

[DOI: 10.22068/ijmse.3284]

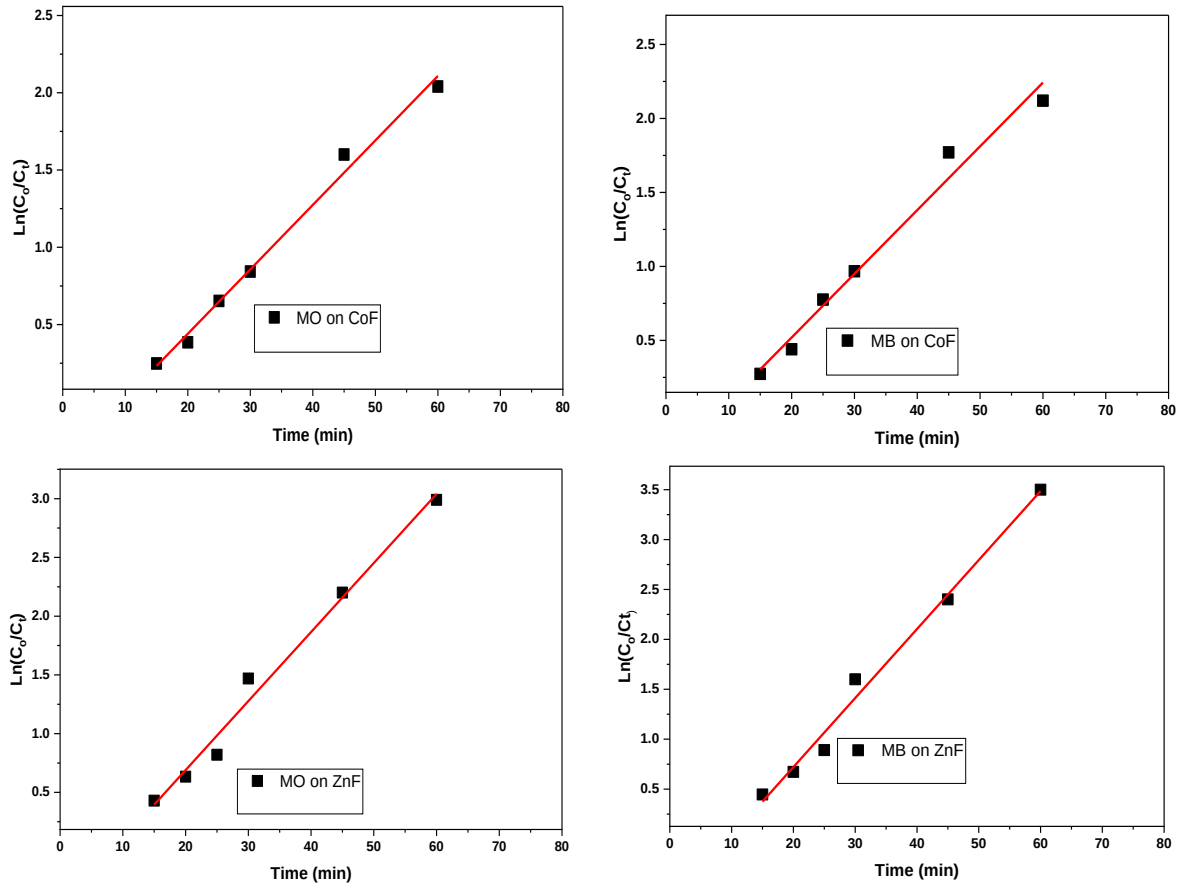

Fig. 8. Ln C_O/C_t vs. the degradation time of MO and MB over ZnF and CoF under sunlight.

These findings confirm that the as-prepared porous $ZnFe_2O_4$ and $CoFe_2O_4$ nanostructures are critical in promoting the degradation of dyes under sunlight instead of UV-vis light lamps that consume/require electrical energy.

On the other side, the photodegradation kinetic was studied [10, 17, 37]. The corresponding slope of the fitting line presents the value of the rate constant k (min^{-1}).

$$\ln\frac{C_0}{C} = kt \quad (3)$$

Where k is the rate constant, t is the time of reaction, Co is the initial concentration, and C is the concentration after irradiation time. Firstly, Plotting Ln(C/Co) vs. time of degradation of MB and MO dyes (Fig. 8) gives a straight line with the slope of the kinetic constant *k,* and that describes the first-order reaction of photocatalytic degradation of dyes. Secondly, reaction half-life time $t_{1/2}$ can be calculated using the following equation:

$$t_{1/2} = 0.693/k \quad (4)$$

Where $t_{1/2}$ is the half-life time of the reaction and k is the rate constant. Fig. 8 demonstrates that the photolysis reaction by CoF and ZnF photocatalysts obeyed the first-order kinetic model and had a best R^2 value approximately equal to unity. Furthermore, we summarized the calculated rate constants and half-lives for the photodegradation reactions of MB and MO dyes using both CoF and ZnF photocatalysts in Table 1.

According to kinetic results, the ZnF photocatalyst showed higher rates and a lower half-time than those of the CoF photocatalyst. This agrees well with the UV-vis spectra and nanosizes calculated by TEM and XRD. Since ZnF has smaller nanoparticles than CoF, it has more active sites.

3.2.3. Mechanism of photocatalytic degradation of MB and MO dyes

The photocatalytic degradation mechanism of MB and MO dyes has been thoroughly suggested. Utilizing both zinc and cobalt ferrites as photocatalysts, the proposed mechanism could be explained by the pairs of hole-electrons in this case.

[DOI: 10.22068/ijmse.3284]

Table 1. Rate constant, half-life, band gap, particle size, and % degradation of dyes.

Dye	sample	K (min^{-1})	$t_{1/2}$ (min)	Band gap (ev)	% removal	Particle size (nm)
MB	ZnF	0.255	2.72	2.24	96.89	9-16
	CoF	0.101	6.86	2.31	92.89	11-18
MO	ZnF	0.772	1.00	2.24	88.41	9-16
	CoF	0.02	5.00	2.31	87.55	11-18

Fig. 9 shows the photocatalytic degradation mechanism of MB and MO dyes over ZnF and CoF photocatalysts. On the other hand, the balanced chemical equations provide an outline of each step in the dye degradation mechanism using ZnF or CoF photocatalysts [11, 15, 22, 26, 28, 34]

$$ZnF \text{ or } CoF + h\nu_{\text{(Sunlight radiations)}} \rightarrow ZnF\ (h^+ + \bar{e}) \text{ or } CoF\ (h^+ + \bar{e}) \quad (5)$$

$$ZnF(h^+) \text{ or } CoF\ (h^+) + 2H_2O \rightarrow ZnF\ (h^+) \text{ or } CoF\ (h^+) + OH^{\bullet} + H^+ \quad (6)$$

$$ZnF\ (h^+) \text{ or } CoF\ (h^+) + OH^- \rightarrow ZnF \text{ or } CoF + OH^{\bullet} \quad (7)$$

$$ZnF \text{ or } CoF + O_{2\ \text{(absorbate)}} + \bar{e} \rightarrow ZnF \text{ or } CoF + O_2^{-} \quad (8)$$

$$OH^{\bullet} + O_2^{-} + (MB) \text{ or } (MO) \rightarrow CO_2 + H_2O \quad (9)$$

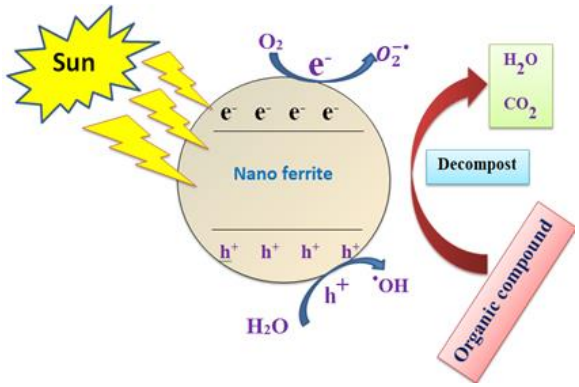

Fig. 9. Mechanism of photodegradation of MB and MO dyes using the ZnF and CoF photocatalysts under sunlight

4. CONCLUSIONS

The degradation of MB and MO dyes was investigated using $ZnFe_2O_4$ and $CoFe_2O_4$ under direct sunlight radiation. The obtained solid ferrites were characterized by XRD, TEM, SEM, UV-vis, and EDS. From XRD and TEM results, the as-prepared ferrites have cubic nanostructures with sizes ranging from 9-16 nm and 11-19 nm for $ZnFe_2O_4$ and $CoFe_2O_4$, respectively. EDS spectra also confirmed that $ZnFe_2O_4$ and $CoFe_2O_4$ were successfully formed with high purity. SEM images showed homogeneous flat surfaces that had porous nanostructures. The photocatalytic degradation findings showed that $ZnFe_2O_4$ outperformed $CoFe_2O_4$ in terms of degradation efficiency (96.89% for MB) and (92.88% for MO) within 60 min. The kinetic study showed a good correlation coefficient for a pseudo-first-order kinetic model. These findings confirmed that the as-prepared $ZnFe_2O_4$ and $CoFe_2O_4$ are promising photocatalysts for environmental water remediation under sunlight instead of UV-vis light lamps that consume/require electrical energy.

FUNDING

The authors declare that no funds, grants, or other support were received during the preparation of this manuscript.

REFERENCES

[1]. Silveira E., Marques PP., Silva SS., Lima-Filho JL., Porto ALF., Tambourgi EB. Selection of Pseudomonas for industrial textile dyes decolourization. International Biodeterioration and Biodegradation. Elsevier; 2009; 63(2): 230–235. Available at: DOI:10.1016/j.ibiod.2008.09.007

[2]. Mathur N., Bhatnagar P., Bakre P. Assessing mutagenicity of textile dyes from Pali(Rajasthan) using Ames bioassay. Applied ecology and environmental research. Citeseer; 2006; 4(1): 111–118.

[3]. Keharia H., Madamwar D. Bioremediation concepts for the treatment of dye containing wastewater: a review. NISCAIR-CSIR, India; 2003; 41(9):1068-75.

[4]. Hu Z., Chen H., Ji F., Yuan S. Removal of Congo Red from aqueous solution by cattail root. Journal of Hazardous Materials. Elsevier; 2010; 173(1–3): 292–297.

[5]. Phalakornkule C., Polgumhang S., Tongdaung W., Karakat B., Nuyut T. Electrocoagulation of blue reactive, red

[DOI: 10.22068/ijmse.3284]

disperse and mixed dyes, and application in treating textile effluent. Journal of environmental management. Elsevier; 2010; 91(4): 918–926.

[6]. Berton G., Gordon S. Modulation of macrophage mannosyl-specific receptors by cultivation on immobilized zymosan. Effects on superoxide-anion release and phagocytosis. Immunology. Wiley-Blackwell; 1983; 49(4): 705.

[7]. Paul BB. Application of natural dyes on textiles - The traditional way in Rajasthan. Colourage. CSIR; 2011; 58(6): 70–72.

[8]. Ezechi EH., bin Mohamed Kutty SR., Malakahmad A., Isa MH. Characterization and optimization of effluent dye removal using a new low cost adsorbent: Equilibrium, kinetics, and thermodynamic study. Process Safety and Environmental Protection. Elsevier; 2015; 98: 16–32.

[9]. Alshorifi FT., Alswat AA., Salama RS. Gold-selenide quantum dots supported onto cesium ferrite nanocomposites for the efficient degradation of rhodamine B. Heliyon. Elsevier; 2022; 8(6), pages E09652.

[10]. Alshorifi FT., Ali SL., Salama RS. Promotional synergistic effect of Cs–Au NPs on the performance of Cs–Au/$MgFe_2O_4$ catalysts in catalysis 3, 4-Dihydropyrimidin-2 (1H)-Ones and degradation of RhB Dye. Journal of Inorganic and Organometallic Polymers and Materials. Springer; 2022; 32(10): 3765–3776.

[11]. Alshorifi FT., Alswat AA., Mannaa MA., Alotaibi MT., El-Bahy SM., Salama RS. Facile and green synthesis of silver quantum dots immobilized onto a polymeric CTS–PEO blend for the photocatalytic degradation of p-Nitrophenol. ACS omega. ACS Publications; 2021; 6(45): 30432–30441.

[12]. Xiong P., Chen Q., He M., Sun X., Wang X. Cobalt ferrite–polyaniline heteroarchitecture: a magnetically recyclable photocatalyst with highly enhanced performances. Journal of Materials Chemistry. Royal Society of Chemistry; 2012; 22(34): 17485–17493.

[13]. Alshorifi FT., El Dafrawy SM., Ahmed AI. Fe/Co-MOF nanocatalysts: greener chemistry approach for the removal of toxic metals and catalytic applications. ACS omega. ACS Publications; 2022; 7(27): 23421–23444.

[14]. Alswat AA., Al-shorifi FT., Ali SL. Preparation of Nanohybrid CuO-Fe_3O_4/Zeolite Nanocomposite as Potential Adsorbent for Toxic As (V) and Pb (II) from Water Solution. Iranian Journal of Materials Science & Engineering. 2022; 19(3).pages 2606

[15]. Mannaa MA., Qasim KF., Alshorifi FT., El-Bahy SM., Salama RS. Role of NiO nanoparticles in enhancing structure properties of TiO_2 and its applications in photodegradation and hydrogen evolution. ACS omega. ACS Publications; 2021; 6(45): 30386–30400.

[16]. Ahmad AI., El-Dafrawy SM., Al-Shorifi FT. Cobalt—Metal-Organic Frameworks (Co-MOFs) nanocatalyst: an efficient catalyst for the preparation of 3, 4-dihydropyrimidinone. Int. J. Nano Mater. Sci. 2017; 6: 25–38.

[17]. Gupta NK., Ghaffari Y., Kim S., Bae J., Kim KS., Saifuddin M. Photocatalytic degradation of organic pollutants over MFe_2O_4 (M= Co, Ni, Cu, Zn) nanoparticles at neutral pH. Scientific reports. Nature Publishing Group UK London; 2020; 10(1): 4942.

[18]. Ahmed J., Alhokbany N., Husain A., Ahmad T., Khan MAM., Alshehri SM. Synthesis, characterization, and significant photochemical performances of delafossite $AgFeO_2$ nanoparticles. Journal of Sol-Gel Science and Technology. Springer; 2020; 94: 493–503.

[19]. Kalam A., Al-Sehemi AG., Assiri M., Du G., Ahmad T., Ahmad I., et al. Modified solvothermal synthesis of cobalt ferrite ($CoFe_2O_4$) magnetic nanoparticles photocatalysts for degradation of methylene blue with H_2O_2/visible light. Results in Physics. Elsevier; 2018; 8: 1046–1053.

[20]. Sharma S., Dutta V., Raizada P., Hosseini-Bandegharaei A., Thakur V., Nguyen V-H., et al. An overview of heterojunctioned $ZnFe_2O_4$ photocatalyst for enhanced oxidative water purification. Journal of Environmental Chemical Engineering.

[DOI: 10.22068/ijmse.3284]

Elsevier; 2021; 9(5): 105812.
[21]. Munir S., Warsi MF., Zulfiqar S., Ayman I., Haider S., Alsafari IA., et al. Nickel ferrite/zinc oxide nanocomposite: investigating the photocatalytic and antibacterial properties. Journal of Saudi Chemical Society. Elsevier; 2021; 25(12): 101388.
[22]. Hammouche J., Gaidi M., Columbus S., Omari M. Enhanced photocatalytic performance of zinc ferrite nanocomposites for degrading methylene blue: effect of nickel doping concentration. Journal of Inorganic and Organometallic Polymers and Materials. Springer; 2021; 31: 3496–3504.
[23]. Khan MAM., Khan W., Ahamed M., Ahmed J., Al-Gawati MA., Alhazaa AN. Silver-decorated cobalt ferrite nanoparticles anchored onto the graphene sheets as electrode materials for electrochemical and photocatalytic applications. ACS omega. ACS Publications; 2020; 5(48): 31076–31084.
[24]. Saleh TS., Badawi AK., Salama RS., Mostafa MMM. Design and development of novel composites containing nickel ferrites supported on activated carbon derived from agricultural wastes and its application in water remediation. Materials. MDPI; 2023; 16(6): 2170.
[25]. Kane A., Assadi AA., El Jery A., Badawi AK., Kenfoud H., Baaloudj O., et al. Advanced photocatalytic treatment of wastewater using immobilized titanium dioxide as a photocatalyst in a pilot-scale reactor: Process intensification. Materials. MDPI; 2022; 15(13): 4547.
[26]. Baaloudj O., Nasrallah N., Kenfoud H., Bourkeb KW., Badawi AK. Polyaniline/Bi12TiO20 hybrid system for cefixime removal by combining adsorption and photocatalytic degradation. ChemEngineering. MDPI; 2023; 7(1): 4.
[27]. Gouda MS., Shehab M., Soliman MM., Helmy S., Salama R. Preparation and characterization of supercapacitor electrodes utilizing catkin plant as an activated carbon source. Delta University Scientific Journal. Delta University for Science and Technology; 2023; 6(1): 255–265.
[28]. Alasri TM., Ali SL., Salama RS., Alshorifi FT. Band-structure engineering of TiO_2 photocatalyst by AuSe quantum dots for efficient degradation of malachite green and phenol. Journal of Inorganic and Organometallic Polymers and Materials. Springer; 2023; volume 33, 1–12.
[29]. Shahzad W., Badawi AK., Rehan ZA., Khan AM., Khan RA., Shah F., et al. Enhanced visible light photocatalytic performance of Sr0.3 (Ba, Mn) 0.7 ZrO_3 perovskites anchored on graphene oxide. Ceramics International. Elsevier; 2022; 48(17): 24979–24988.
[30]. Baaloudj O., Kenfoud H., Badawi AK., Assadi AA., El Jery A., Assadi AA., et al. Bismuth selenide crystals as recent photocatalysts for water treatment and energy generation: A critical review. Catalysts. MDPI; 2022; 12(5): 500.
[31]. Yassin AY., Abdelghany AM., Salama RS., Tarabiah AE. Structural, Optical, and Antibacterial Activity Studies on CMC/PVA Blend Filled with Three Different Types of Green Synthesized ZnO Nanoparticles. Journal of Inorganic and Organometallic Polymers and Materials. Springer; 2023;33, 1–13.
[32]. Gouda MS., Shehab M., Helmy S., Soliman M., Salama RS. Nickel and cobalt oxides supported on activated carbon derived from willow catkin for efficient supercapacitor electrode. Journal of Energy Storage. Elsevier; 2023; 61: 106806.
[33]. Mostafa MMM., Alshehri AA., Salama RS. High performance of supercapacitor based on alumina nanoparticles derived from Coca-Cola cans. Journal of Energy Storage. Elsevier; 2023; 64: 107168.
[34]. Lee HJ., Kim JH., Park SS., Hong SS., Lee GD. Degradation kinetics for photocatalytic reaction of methyl orange over Al-doped ZnO nanoparticles. Journal of Industrial and Engineering Chemistry. Elsevier; 2015; 25: 199–206.
[35]. Robles-Águila MJ., Luna-López JA., Hernández De La Luz ÁD., Martínez-Juárez J., Rabanal ME. Synthesis and characterization of nanocrystalline ZnO doped with Al^{3+} and Ni^{2+} by a sol–gel method coupled with ultrasound

[DOI: 10.22068/ijmse.3284]

irradiation. Crystals. MDPI; 2018; 8(11): 406.

[36]. Mahdavi R., Talesh SSA. Sol-gel synthesis, structural and enhanced photocatalytic performance of Al-doped ZnO nanoparticles. Advanced Powder Technology. Elsevier; 2017; 28(5): 1418–1425.

[37]. Yao Y., Cai Y., Lu F., Qin J., Wei F., Xu C., And Wang, S. Magnetic $ZnFe_2O_4$–C_3N_4 hybrid for photocatalytic degradation of aqueous organic pollutants by visible light. Industrial & Engineering Chemistry Research. ACS Publications; 2014; 53(44): 17294–17302.

[DOI: 10.22068/ijmse.3284]